Geomorphology 445 (2024) 108972

Contents lists available at ScienceDirect

Geomorphology

journal homepage: www.journals.elsevier.com/geomorphology

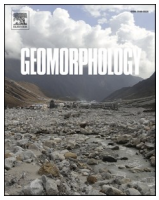

Secular shoreline response to large-scale estuarine shoal migration and welding

Marine Vandenhove [a,b,*], Bruno Castelle [a], Alexandre Nicolae Lerma [b], Vincent Marieu [a], Ema Dalet [b], Vincent Hanquiez [a], Vincent Mazeiraud [c], Stéphane Bujan [a], Cyril Mallet [b]

[a] Univ. Bordeaux, CNRS, Bordeaux INP, EPOC, UMR 5805, F-33600 Pessac, France
[b] BRGM (French Geological Survey), Direction Régionale Nouvelle-Aquitaine, Parc Technologique Europarc, 24 avenue Léonard de Vinci, Pessac 33600, France
[c] Communauté de Communes Médoc Atlantique, 9 rue du Maréchal d'Ornano, Soulac-sur-Mer 33780, France

ARTICLE INFO

Keywords:
Coastal erosion
Estuary mouth
Shoal welding
Bathymetric control
Multidecadal variability

ABSTRACT

The 14.5-km North-Médoc coast, southwest France, is a high-energy meso- to macro-tidal environment adjacent to the largest estuary in Europe. Over the last centuries, this coastline has locally suffered periods of severe erosion, threatening coastal infrastructures and requiring the progressive implementation of coastal structures and, more recently, localized beach nourishments. This contribution combines 84 years (1937–2021) of shoreline data from various sources, 118 years (1903–2021) of shallow water bathymetric surveys and historical photographs. Results show that, averaged in both time and space, the coast eroded by −0.6 m/yr over the last 84 years, but with a large alongshore and temporal variability. Erosion is locally peaking at −5.2 m/yr, while accretion is restricted to a remote 2.5-km and locally peaks at 5.4 m/yr. A salient characteristic of shoreline evolution is the alternation of rapid erosion (< −5 m/yr) and dramatic accretion (> 20 m/yr) periods over relatively short intervals (≈ 10 years) and across limited alongshore distances (e.g. couple of kilometers). We show that shoreline change is mainly driven by offshore shoal dynamics originating from the estuary mouth further migrating in both the cross-shore and longshore direction. Two major events occurring at different times and locations, leading to volumetric changes of the order of millions to tens of millions cubic meters are analysed. The first attachment, completed around the 1920s, supplied nearly 5-million m^3 of sediment, widening and rising the beach by hundreds of meters and meters, respectively. This shoreline bulge subsequently diffused and migrated downdrift, resulting in a quasi-steady erosion rate of approximately −3.3 m/yr. The second shoal attachment, which started around the 1950s, first stopped the chronic erosion observed in the northern sectors, and subsequently drove dramatic (> 500 m) shoreline accretion in the 1970s. Current yearly small-scale beach nourishments only temporally buffer erosion, while a mega-nourishment with similar scales as the first shoal attachment could provide a more sustainable solution. We anticipate that this study, together with future modelling work will help the coastal managers and decision makers to optimize their coastal management strategy.

1. Introduction

Approximately one third of the ice-free coasts are made of sand (Luijendijk et al., 2018), with sandy shores being particularly vulnerable to coastal erosion. Sandy coasts show large morphological changes with erosion and accretion periods alternating on short- (days-to-weeks), medium- (months-to-decades) and long-term (> decades) timescales (Stive et al., 2002). Severe erosion can occur under a given storm or series of storms (Masselink et al., 2016; Harley et al., 2017). Erosion can also be long-lasting, with chronic erosion potentially requiring to permanently move people or infrastructures out of harm's way (managed retreat, Dundon and Abkowitz, 2021). It is thus increasingly important for coastal managers and decision makers to improve the understanding of past and future sandy coast evolution. This is particularly true for sandy coasts adjacent to estuary mouths, which are often focal points for coastal development and human recreation. Such environments are also the coastal sectors often showing globally the largest shoreline time and space variability (Bamunawala et al., 2021; Castelle et al., 2022).

Temporal changes of sandy coasts can be affected by human

* Corresponding author at: Univ. Bordeaux, CNRS, Bordeaux INP, EPOC, UMR 5805, F-33600 Pessac, France.
E-mail address: marine.vandenhove@u-bordeaux.fr (M. Vandenhove).

https://doi.org/10.1016/j.geomorph.2023.108972
Received 9 June 2023; Received in revised form 3 November 2023; Accepted 3 November 2023
Available online 10 November 2023

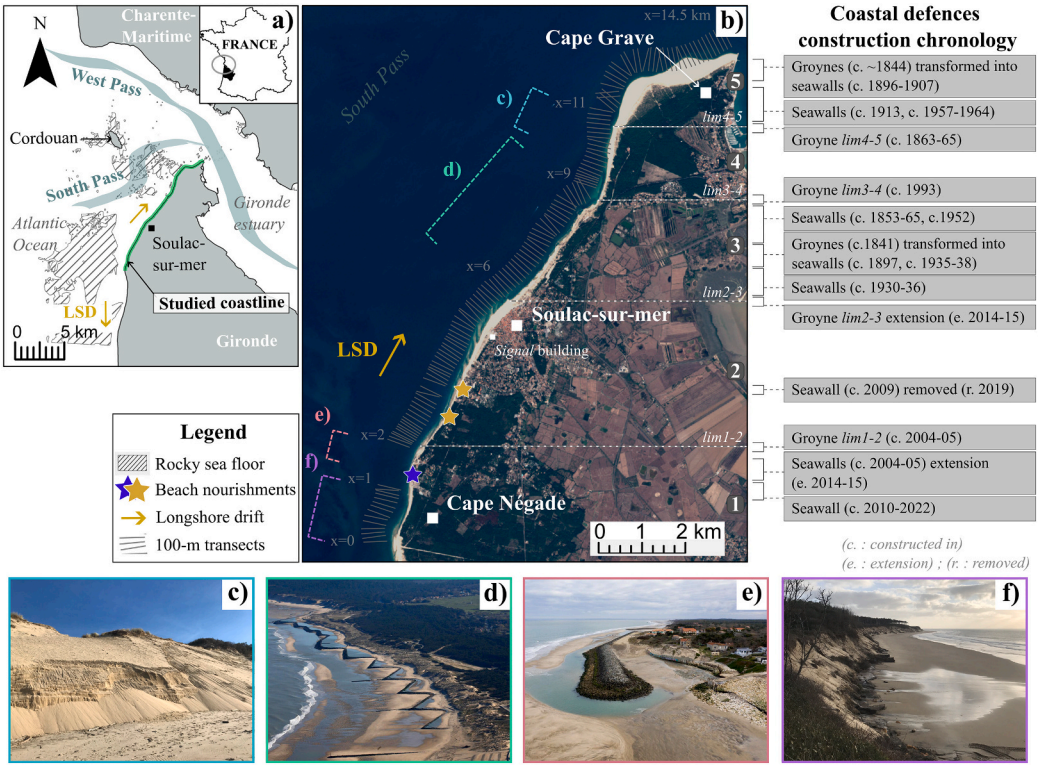

Fig. 1. (a) Location map of the study area, and rocky outcrops, zoomed in (b) showing coastal defence (with construction dates) beach nourishment locations, the 100-m transects along which shoreline is extracted, and the local longshore coordinate system (Sentinel 2 on September 20, 2022). The five distinct sectors used to describe in the text the alongshore variability of shoreline response are shown by the dotted white line. Photographs of (c) a coastal dune under chronic erosion (Ph. M. Vandenhove - feb. 2022), (d) coastal defences from mid-20th century (@L. Theillet), (e) coastal defences north of Cape Négade (@G.Bonnaud) and (f) northern side of Cape Négade where severe chronic erosion depleted the coastal dune system and left the coastal forest directly exposed to marine erosion (Ph. M. Vandenhove - jan. 2022).

interventions including coastal structures and beach nourishments (Hamm et al., 2002; Ells and Murray, 2012; de Schipper et al., 2021). Nevertheless coastal response is often mostly driven by natural external forcing, that is, by variability in tide and incident wave conditions operating on a wide range of timescales (Castelle and Masselink, 2023). Shoreline variability becomes increasingly complex when approaching tidal inlets and estuary mouths as it is driven by an interplay between external (e.g. waves) and internal (e.g. ebb tidal delta cycles) factors (e.g. FitzGerald, 1984). Channel dredging for navigation purposes can also affect the morphodynamics of the system (Zarzuelo et al., 2019). On the longer term, sea-level rise and terrestrial (e.g., fluvial sediment supply) processes that govern the local sediment budget can also be important to shoreline change of adjacent coasts (Bamunawala et al., 2021).

Ebb-tidal delta sandy shoals typically successively form, migrate (Ridderinkhof et al., 2016b) and weld to the shore under the combined action of wave- and tide-driven currents (De Swart and Zimmerman, 2009; Ridderinkhof et al., 2016a). Such quasi-cyclic internal behaviour includes hooked sand ridge welding to the updrift coast (Hine, 1979; Robin et al., 2009), where updrift and downdrift refer to the dominant longshore sand transport at the scale of the system. Closure and opening of tidal channels at the most wavedominated environments can also be observed (Fortunato et al., 2014). In addition, critical to shoreline variability along the downdrift coast is shoal attachment to the shore (Gaudiano and Kana, 2001; Ridderinkhof et al., 2016a; Elias et al., 2019; Burvingt et al., 2022). Such shoal attachment to the downdrift coast can be viewed as a local, natural, beach nourishment as the bulge of sand subsequently diffuse and migrate downdrift (Van den Berg et al., 2011). A local longshore drift reversal can be locally observed along the downdrift coast as a result of wave refraction around the ebb-tidal delta (e.g. Hayes et al., 1970) and/or change in shoreline orientation (e.g. Idier et al., 2013).

So far studies addressing the evolution of such downdrift coastal sectors mostly focused on relatively small inlet systems (e.g. Gaudiano and Kana, 2001), which are often made by a single channel and characterized by a shoreline variability occurring on shorter time and space scales (e.g. Byrne et al., 1980; FitzGerald, 1982). Such smaller-scale systems are thus generally easier to monitor. In contrast, close to large-scale inlets and estuary mouths, shoreline changes can occur on hundreds of meters in the cross-shore direction, along kilometers to tens of kilometers of coastline and on decadal time scales (FitzGerald, 1982; Burvingt et al., 2022; Castelle et al., 2022). This challenges the monitoring, understanding and modelling of shoreline change of such downdrift coast environments. Because in situ monitoring programs are scarce and tedious, optical satellite imagery is an appealing avenue to cope with large-scale inlet and downdrift shoreline dynamics (e.g. Warrick et al., 2023). However, on high-energy gently sloping tidal beaches the instantaneous shoreline is largely dependent on water level variation and beach slope (Vos et al., 2019b, 2023), and satellite-derived shoreline errors can thus exceed 50 m (Konstantinou et al., 2023). Ocean colour depth inversion (e.g. Lubac et al., 2022) is also not possible for turbid water. This therefore challenges the use of optical satellite imagery for high-energy meso-macrotidal and turbid water inlet environments. The welding of shoal originating from such large-scale tidal inlets or estuary mouths, which can result in sand input on the order of hundred cubic meters per beach width (Burvingt et al., 2022), can also be viewed as a natural analogy of a 'mega-nourishment'. Such meganourishment (e.g. Sand Engine, de Schipper et al., 2016), which is performed in a single operation, contrasts with quasi-periodic (e.g. yearly) traditional beach nourishments. Such approach can be thus an efficient management strategy on sediment-starving sectors at the scale of a coastal cell (Roest et al., 2021).

The 14.5-km North-Médoc coast sector, southwest France, is

adjacent to the largest estuary in Europe (Fig. 1a). It is a meso to macrotidal, turbid water, energetic environment which, over the last centuries, has suffered periods of severe erosion. This required the establishment of coastal protections since the mid-19th century, including riprap seawalls and groynes, and more recently localized beach nourishments. Despite all these measures, some urbanized and state forest sectors are still largely threatened by erosion. A mega-nourishment project is also currently debated to safeguard this territory, without having insight into its potential lifetime. Despite the strong need of the coastal managers and decision makers to better understand coastal change and their primary drivers to guide their future coastal management strategy, there is a strong lack of scientific literature on this area. Howa (1997) tentatively designed a conceptual model of the Gironde estuary mouth based on the orientation of offshore mega-ripples, which was further completed by Mallet et al. (2000), with none of the studies addressing shoreline change. This study therefore aims at providing new and quantitative insight into secular shoreline change along this coastline linked with the welding of shoals circulating across the ebb delta and to further discuss the implications from the perspective of coastal management. For this purpose, different shoreline, topographic and bathymetric programs are combined.

2. Study site

The study site covers approximately 14.5-km of north-northeast facing sandy coastline on the North-Médoc coast, from Cape Grave to Cape Négade (Fig. 1b). It is exposed to seasonally-modulated energetic waves generated in the North Atlantic. According to measurements and numerical hindcasts, at a location < 100 km south of our study site in approximately 50-m depth, waves vary from a dominant W-NW (W) direction in July (January) with a monthly-averaged significant wave height of 1.11 m (2.40 m) (Castelle et al., 2017). Given the larger and shallower continental shelf and the presence of complex underwater rocky outcrops offshore, wave conditions at our study site are typically less energetic at the coast than further south. Another important characteristics is the strong latitudinal gradient, within the study site, in incident wave energy with breaking wave height progressively decreasing northwards. The dominant angle of wave incidence drives a net longshore drift directed northeastwards (Idier et al., 2013; Howa, 1997), diverging from the southward longshore drift further south. The North-Médoc beaches are adjacent to, and downdrift of, the Gironde estuary (Fig. 1a). The tide is semi-diurnal, meso-macrotidal, with a tidal range from 1.5 m at neap tide to 5.5 m at spring tide (Castaing and Allen, 1981) leading to tide-driven currents with a maximum bottom velocity up to 1 m/s near the coast (Howa, 1987).

The Gironde estuary is the largest estuary of the Atlantic coast of Europe, with a maximum cross section of 12 km at high tide near the mouth (Castaing and Allen, 1981). It is a large-scale mixed energy inlet (Allen, 1991). The average yearly suspended sediment and water discharges are 2.5 10^6 t/an (Jouanneau et al., 1999) and 900 m^3/s (Sottolichio and Castaing, 1999), respectively. From 2005 to 2014, this value decreased to 680 m^3/s due to changes in hydrological conditions (Jalón-Rojas et al., 2015). The estimated volume of water flowing through the inlet, i.e. tidal prism, is 1.1 10^9 m^3 and 2 10^9 m^3 at neap and spring tide, respectively (Allen et al., 1974a). The inlet is divided into two main channels (Fig. 1a). The northern one is called the *West Pass*, which is located between the rocky platform of Cordouan and the Charente-Maritime coast. This 15–30 m deep navigable channel is maintained with frequent dredging operations. The secondary channel (10–20 m deep), called the *South Pass*, is located in the south of the estuary mouth and has been reasonably stable in time. It deviates from the main channel in front of the Cordouan platform to the downdrift sector of the inlet constrained by the presence of several rocky outcrops (see Fig. 1a). In addition to regular dredging operation of the *West Pass*, aggregate extraction has also been performed since approximately 1945 at different locations of the estuary mouth.

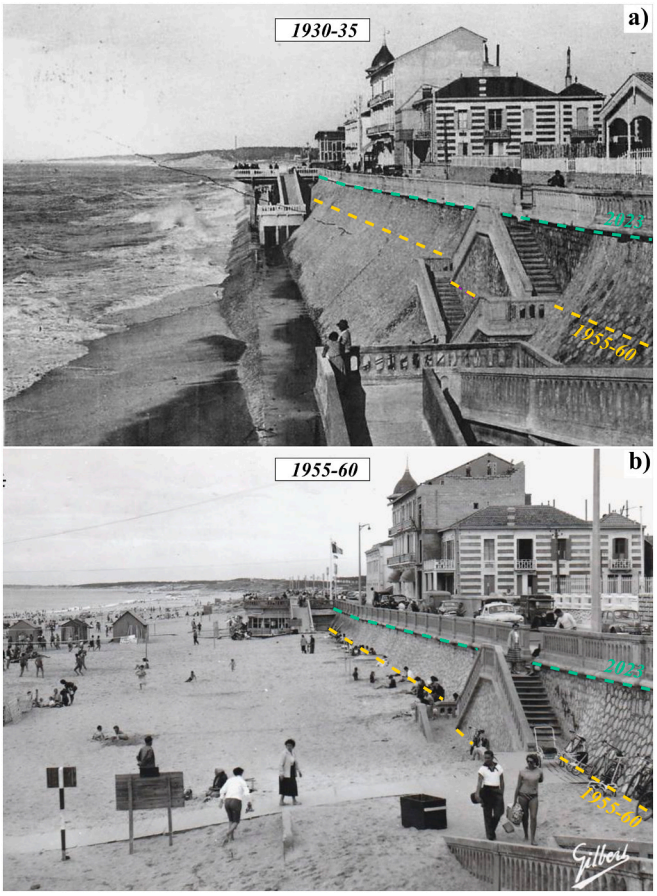

Fig. 2. Historical photographs of Soulac-sur-Mer seafront a) in the early 1930s and b) late 1950s, showing the dramatic elevation and widening of the beach. In the 1930s, the beach level was at the foot of the sea wall. This sandy beach rose several meters to reach the yellow dotted line in the late 50s. In 2023, the beach level is at the cyan dotted line. (For interpretation of the references to colour in this figure legend, the reader is referred to the web version of this article.)

Since the sea level stabilization at ca. 6000 BP, there is evidence that the North-Médoc beaches have been eroding since at least ca. 3500 BP as shown by sedimentological and archeological analysis (Stéphan et al., 2019). More recently, from the 1700s to the early 1900s historical charts also indicate widespread erosion of the entire coastline, with erosion rates increasing northwards (Lévêque, 1936; Allen et al., 1974b; Howa, 1987). The authors reported continuous erosion over these 2 centuries, without apparent recovery period. Since the mid-19th century, with recreational development, the study site has become more attractive and leaded to large urban expansion. A wide range of coastal defences have been progressively constructed to protect the coast against erosion. The first structures were made of groynes built in 1841 within Sector (3) (Fig. 1b). Later on, the series of groynes were progressively transformed into a continuous seawall between 1853 and 1938. This transformation was characterized by several reconstructions due to storms and bombing (World War II). Subsequently, additional seawalls were built in the same sector, extending the length of the original seawall to span approximately 3 km of coastline. The current boundaries of this seawall are marked by two groynes, referred to as lim*3–4* and groyne lim*2–3* in Fig. 1d) covering the entire Sector (3). At the northern end, groyne *lim3–4* was established in 1993, while at the southern end groyne *lim2–3* was initially built in 1935, but was repaired further extended in 2014–2015 after the extreme winter of 2013/14 (Fig. 1b). Another groyne constructed between 1863 and 1865 delimits Sector (5) and Sector (4) (i.e. groyne lim*4–5*). Finally, additional seawalls which were

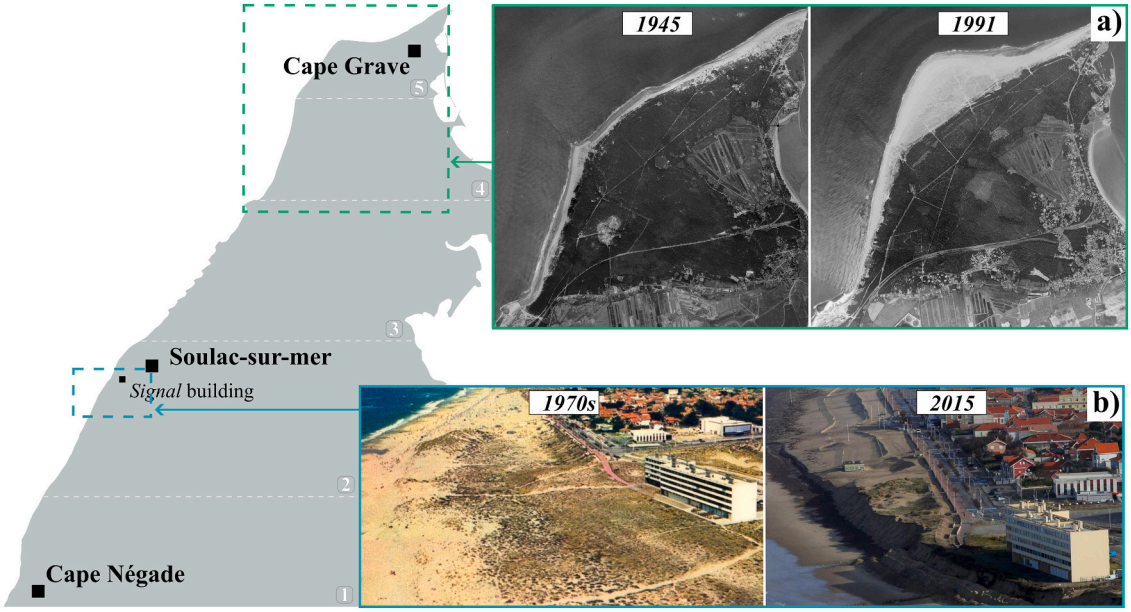

Fig. 3. Historical aerial photographs illustrating the large-scale shoreline evolution, accreting sector in the north (1945–1991) and eroding sector south of Soulac-sur-Mer, in front of the *Signal building* (1970s-2015). (Ph. 1970s, source unknown; Ph. 2015,@L.Theillet).

built at Cape Grave during the 20th century are now buried under the sand. Photograph archives indicate that, during the 20th century, large shoreline and coastal landscape changes have been observed with rapid erosion and accretion periods alternating over time and space. In Sector (2), at Soulac-sur-Mer, between the 1930s and 1950s, the beach elevation rose by several meters (Fig. 2). It is important to note that other photographs from other view points taken in the 1910s (not shown) indicate that at that time the beach was even lower than in 1930s by a few meters, highlighting the worrying erosive situation in the early 20th century. Two decades later, in the 1970s, 2 km south of Soulac-sur-Mer, aerial photographs show the presence of a 200-m wide vegetated dune in front of the Signal building that entirely eroded over 45 years while simultaneously, the northern sector (5) has been accreting locally by hundreds of meters (Fig. 3). In the early 21th century, riprap seawalls and groynes have been erected to protect the more exposed urban areas, in Sector (1). Since 2018, localized beach nourishments (around 60 10^3 m^3/yr) have been performed every year along some of the most vulnerable areas (Sector (2)) to buffer incident wave energy, while non-documented nourishments of similar scale were irregularly performed further south in Sector (1) since the early 2000s (Fig. 1b). Despite all these measures, some of the areas of the North-Médoc coast are still under chronic erosion, threatening infrastructures, some urbanized (Fig. 1e) and state forest areas (Fig. 1c; f), while other are accreting (Fig. 3).

3. Methods

3.1. Shoreline data sources

In order to address the alongshore variability of shoreline response, we tailored a local coordinate system spanning from 0 km at the southern boundary of the study area to 14.5 km at the northern end. The coastline was further divided into 100-m spaced transects (Fig. 1b), along which shoreline position was further interpolated from several data sources. The shoreline interpolation at each 100-m spaced transect was performed when the data distance from the transect was under 300 m. The shoreline dataset used herein combines four different sources, with different temporal coverage, accuracy and frequency, namely: i) aerial photo interpretation, ii) satellite-derived shoreline, iii) in situ shoreline surveys and iv) topographic surveys. These datasets are all described below.

i. Aerial photo interpretation

From 1937 to 2020, 41 orthophotos were gathered from several sources, covering partially or entirely the study site (Table 1). In total, 38 orthophotos were georeferenced orthomosaics from aerial photos, while three were georeferenced satellite optical images from FORMOSAT2 (Lafon et al., 2010). Amongst the 38 aerial photo orthomosaics, 15 were already merged and orthorectified with a conservative error under 5 m (Castelle et al., 2018). Another 23, from 1945 to 2010, were retrieved from the French National Geographical Institute (IGN).

Table 1
Number of data (*N*) available for each data source used in this study, with their temporal (year) and mean spatial (percent) coverage. The shoreline proxy and errors are provided.

Data protocol	N	Temporal cover. (yr)	Spatial cover. (%)	Proxy	Source	Error (m)
Photo-interpretation	41	1937–2020	95 %	Dune foot	Aerial photos series, LiDAR, satellite images	RMSE <5 m
Satellite-based Shoreline	1404	1984–2021	20 %	Water line	CoastSat toolkit[a], L5, L7, L8 and S2	>30 m[b]
surveys	14	2014–2022	85 %	Dune foot	GNSS surveys[c]	Mean error <2 m
Topographic surveys	14	2013–2021	65 %	Dune foot	GNSS surveys[d]	–

[a] Vos et al. (2019b).
[b] Castelle et al. (2021).
[c] Castelle et al. (2015).
[d] CDCMA (2021a).

These 23 orthophotos were assembled by a photogrammetry software (Agisoft Metashape 1.7.2) and transformed into 23 3D models to generate orthomosaics following the approach detailed in Laporte-Fauret et al. (2022). The obtained mean horizontal RMSE is 1.9 m, with a maximum of 4.9 m for the orthomosaics with the poorest quality (1947). On a GIS Software (ArcGIS Desktop 10.6), the shoreline position was then manually digitized by an operator. The dune foot and the limit of vegetated foredune were used as proxies for the shoreline position for eroding and accreting sectors, respectively. In case of dike/seawall and absence of established or incipient dune, the foot of the coastal infrastructure was considered as the shoreline. In order to estimate the uncertainty associated to operator interpretation, five operators manually retrieved the shoreline position on two orthomosaics with the poorest (1937) and best (2010) resolution and light exposure. The shoreline retrieved by the first author was kept for the analysis. Operator-derived shoreline differences were the largest in accreting sectors as the bare sand/vegetation limit is blurred due to the sparse vegetation coverage of the incipient foredune. The overall RMSE due to operator interpretation is 5.1 m for 2010 and 17.5 m for 1937. In eroding sectors this RMSE is only 2.7 m and 6.8 m in 2010 and 1937, respectively. It peaks locally at 18.5 m in 2010 in an accreting sector with the presence of incipient foredune. For the orthomosaic of 1937, the errors locally well exceed 50 m where two operators detected the former dense vegetation limit instead of the more subtle limit of incipient vegetation. This was due to a recent shoreline accretion by tens to hundreds of meters due to a large-scale shoal welding to the coast (see Results section).

ii. Satellite-derived shorelines

The open-source CoastSat software developed by Vos et al. (2019a) was used to infer shoreline position from 1984 to 2021. This toolkit uses the Google Earth Engine satellite database composed of satellite images coming from Landsat 5, 7, 8, and Sentinel-2 campaigns. The 14.5-km coastline was divided into 6 boxes segments where satellite images were extracted, on which the toolbox applied generic shoreline detection algorithm to extract the instantaneous sand/water interface (referred to as waterline proxy for this data source). This resulted in 1404 3-km long waterline segments, in 6 overlapping boxes (Table 1). Beaches are gently sloping meso-macrotidal and exposed to high-energy waves, therefore so the satellite-derived shoreline errors exceed 30 m (Castelle et al., 2021; Konstantinou et al., 2023; Vos et al., 2023). Contrary to Castelle et al. (2021), tide and run-up correction allowing to decrease errors to approximately 10 m was not applied. The two primary reasons are that beach slopes varies alongshore at our study site and that, in line with Castelle et al. (2022), such uncorrected satellite-derived shoreline dataset is enough to provide insight into the large-scale spatial and temporal patterns of shoreline change.

iii. Shoreline surveys

From 2014 to 2022, twice a year, shoreline position was surveyed in situ along the 110 km of the Gironde coast, comprising our study site, typically before (November) and after (April) the winter. An all-terrain vehicle (ATV), equipped with a Post-Processed Kinematic Global Navigation Satellite System (PPK GNSS), is used to survey the shoreline from south to north between low and mid-tide. Dune foot and incipient foredune vegetation are used as shoreline proxy in eroding and accreting sectors, respectively. The monitoring and post-processing strategies, which provide continuous shoreline position with an estimated 3-m accuracy, are detailed in Castelle et al. (2015). Importantly, the northern extremity of the field site ($x > 11$ km, nearly 15 %) was not systematically surveyed as erosion cliffs and outcropping coastal structures often limit the ATV access to this part of the coast.

iv. Topographic surveys

From 2013 to 2021, 14 topographic surveys were performed (CDCMA, 2021a), using an ATV equipped with a centimetric Real-Time Kinematic (RTK) GNSS system. These surveys followed the 100-m spaced transects (see Fig. 1b) over 65 % of the 14.5-km coastline, mostly in the southern part of the study site (Table 1). As the surveyed sector essentially covers eroding coastline, the dune foot position was easily depicted from the beachdune profile as the location of the slope break.

Table 2
Bathymetric dataset characteristics in terms of spatial coverage (Partial, Medium or Wide, see examples in Fig. 4), number of probes and their distribution, transect spacing and data source.

Date	Spatial coverage	Number of probes (n)	Probes distribution	Distance between transects (m)	Source
1903	Partial	2387	Medium	300	GPMB* archives
1909	Partial	2346	Medium	300	GPMB* archives
1917	Partial	3357	Medium	300	GPMB* archives
1920	Partial	3587	Medium	250	GPMB* archives
1921	Partial	4033	Medium	250	GPMB* archives
1922	Partial	4196	Medium	250	GPMB* archives
1926	Medium	4631	Medium	250	GPMB* archives
1928	Medium	5821	Medium	250	GPMB* archives
1929	Medium	5163	Medium	250	GPMB* archives
1931	Medium	4391	Medium	250	GPMB* archives
1932	Medium	5535	Medium	250	GPMB* archives
1933	Medium	5791	Medium	250	GPMB* archives
1934	Medium	3728	Medium	250	GPMB* archives
1935	Medium	4249	Medium	250	GPMB* archives
1936	Medium	4243	Medium	250	GPMB* archives
1937	Medium	4790	Medium	250	GPMB* archives
1938	Medium	5045	Medium	250	GPMB* archives
1939	Medium	4814	Medium	250	GPMB* archives
1959	Medium	3899	Medium	300	GPMB* archives
1984	Wide	5204	Sparse	300	GPMB* archives
1993	Partial	1975	Sparse	200	GPMB* archives
2000	Partial	5017	Medium	300	GPMB* archives
2019	Wide	1,832,082	Dense	300	Single beam sounder measures
2021	Wide	928,865	Dense	300	Single beam sounder measures

* Grand Port Maritime de Bordeaux (Bordeaux Harbour).

3.2. Bathymetric data and interpolation

A total of 25 bathymetric surveys covering the southern part of the estuary mouth were collected from 1903 to 2021 (Table 2), with 23 datasets from 1903 to 2000 being bathymetric paper charts coming from Bordeaux Harbour (Grand Port Maritime de Bordeaux, GPMB) archives. They were scanned and uploaded in a GIS Software (i.e. ArcGIS Desktop 10.6) to be georeferenced and further digitized. For the most recent data, the chart grid coordinates were used for georeferencing. The process was different for older datasets since they had no coordinate

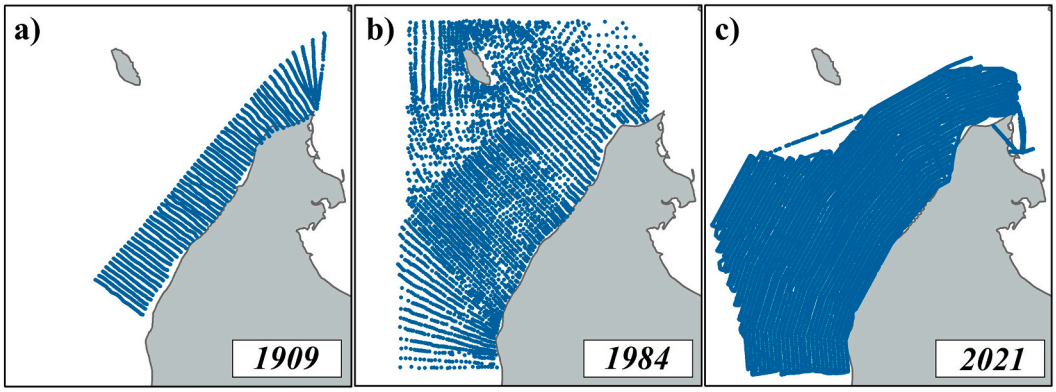

Fig. 4. Illustration of the three primary survey data spatial coverage and probe distribution: a) partial coverage and medium probe density; b) wide coverage and sparse probe density; c) wide coverage and dense probe distribution.

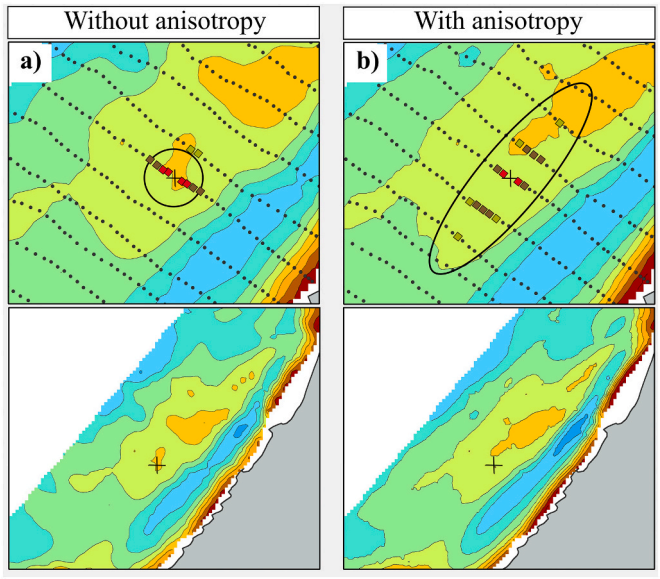

Fig. 5. Example of the weight each data will have in the interpolation process depending of their spatial distribution a) without anisotropy and b) with an anisotropic interpolation. Data in red have a strong impact in the interpolation while green ones have less, brown data being the average. (For interpretation of the references to colour in this figure legend, the reader is referred to the web version of this article.)

system visible on the map. Instead, historical reference points were used, such as lighthouses, churches and crossroads, with a minimum of 10 points homogeneously distributed over each chart. For every chart, each bathymetric probe was then manually digitized. Spatial coverage was either partial, medium or wide while the probes density went from sparse to medium (e.g. Fig. 4a,b). The two latest datasets (i.e. 2019 and 2021) come from bathymetric survey campaigns carried out using a single-beam sounder (CDCMA, 2021b). These surveys uniformly cover the entire study area with high point density (Fig. 4c). Except for these 2019 and 2021 datasets, the data were collected along approximately 250–300-m spaced cross-shore transects (Fig. 4a,b, Table 2), while within the transects, data points are separated by approximately 50 m. This distribution can lead to spurious spatial oscillations after interpolation, resulting in a bathymetric map deviating from reality and flawed/noisy difference plots. Given that the morphology of the offshore banks and channels are more longshore than cross-shore oriented, an anisotropic IDW (Inverse Distance Weighted) interpolation method was used in order to give more weight in the interpolation to the values of adjacent transects, as represented in Fig. 5. This anisotropic interpolation was carried out with a 800 m long and 200 m wide search ellipsoid, using a weighted average of 10 to 15 neighboring data points within the searching area (Fig. 5b). Finally, the location of the offshore rocky outcrops were provided by SHOM - Service Hydrographique et Océanographique de la Marine, 2005.

4. Results

4.1. Shoreline evolution since 1937

Fig. 6a shows the time and space evolution of the 14.5-km North-Médoc coastline since 1937 using the dune foot proxy dataset given in Table 1 and by discriminating five distinct alongshore sectors.

The first sector (1) (Fig. 6d) at $0 < x < 1.5$ km shows an average shoreline retreat of 329 m, increasing northwards, with a maximum of 440 m and minimum of 128 m. This corresponds to an erosion rate ranging from 5.2 m/yr ($x = 1.1$ km, the most rapidly eroding location of the entire coastline) to 1.5 m/yr, with a mean of 3.9 m/yr (see Fig. 6b showing the alongshore distribution of mean shoreline trend at each transect).

Within Sector (2), from $x = 1.5$ km to Soulac-sur-Mer seafront ($x = 6.1$ km), the time average shoreline erosion was relatively uniform alongshore at $1.5 \text{ km} < x < 5.6$ km (Fig. 6b). At $x = 5.6$–6.1 km, Soulac-sur-Mer seafront, the mean erosion rate decreased to 0.6 m/yr. Of note (not shown), at this location, the shoreline position measured in situ and derived from aerial photograph was relatively stable from 2014 to 2022. In contrast, at the same location, the satellite-derived waterline migrated seaward at a mean rate of 10.9 m/yr during this period. This emphasizes the impact of the Sector (2) northern groyne lim*2–3* (Fig. 1b), which trapped the dominant northerly longshore drift, driving the rapid widening of the beach. Overall, an average shoreline retreat by 231 m (−2.7 m/yr) occurred within Sector (2). Erosion was, however, not steady which is further emphasized in Fig. 7a showing the temporal evolution of shoreline position at this location. From 1947 (Fig. 7c) to 1957 (Fig. 7d), a localized accretion by approximately 70 m was observed (d1 in Figs. 7a,d), followed by decades of chronic erosion. Although barely visible on the time stack due to the colour scale (Fig. 6a), this accretion explains the large beach rise photographed at this location (Fig. 2).

Within Sector (3), from the groyne *lim2–3* at $x = 6.1$ km, to the groyne lim*3–4* (Fig. 1b) at $x = 9.3$ km, the shoreline accreted on average by 37 m (i.e. mean accretion of approximately 0.4 m/yr). This shoreline accretion is the signature of the vegetated dune benefiting from the protection of the 3-km long seawall constructed in 1938 along this sector (Fig. 1d).

Within Sector (4), between the groyne *lim3–4* ($x = 9.3$ km) and the groyne lim*4–5* ($x = 11.1$ km) (Fig. 1b), a slow erosion (48 m, 0.6 m/yr) and a slow accretion (19.5 m, 0.2 m/yr) is observed in the south and in

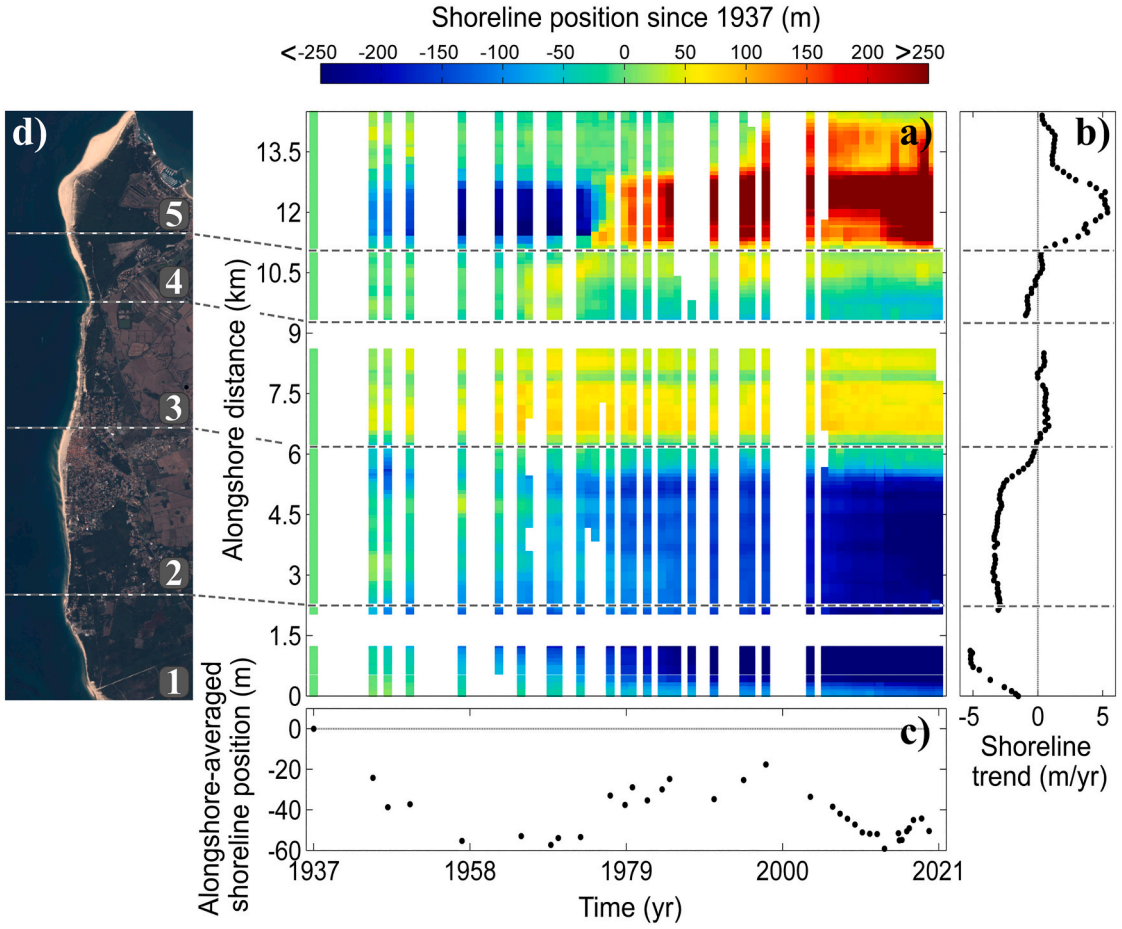

Fig. 6. (a) Time stack of shoreline change and (b) corresponding alongshore distribution of mean shoreline trend, calculated with end point method (c) and time series of alongshore-averaged shoreline position. In (a,b) the horizontal dotted lines indicate the location of the major groynes progressively erected since the 19th century, which are further used to define the different coastal sectors described in the text. (d) Satellite image (Sentinel 2 on September 20, 2022) showing the location of the five sectors.

the north, respectively. However, shoreline trajectory changes were also observed in time, with an accretion of 54 m followed by the same erosion from 1962 to 1977 around $x = 10$ km (Fig. 7a).

In the most northern sector (5), from the groyne *lim4–5* ($x = 11.1$ km) to Cape Grave ($x = 14.5$ km)(Fig. 1b), dramatic shoreline changes were observed. Four periods can be distinguished: (i) three decades of severe erosion between 1937 and 1970 at an average rate of 3.6 m/yr followed by (ii) three decades of strong accretion starting in the 1970s with shoreline advancing by 307 m at a mean rate of 11.0 m/yr, and with shoreline position largely exceeding the 1937 shoreline position after 1977 (Fig. 6a). Between 1998 and 2010 (iii) a second erosion period (2.6 m/yr) took place, followed by (iv) another accretion period (17.9 m/yr). In total, this sector averaged alongshore accretion was 217 m of vegetated dune with a rate of 2.6 m/yr between 1937 and 2021. However, changes were not uniform alongshore, with a presence of a large shoreline bulge (Fig. 8a) which slightly diffused and migrated northeastwards (Fig. 8a).

When integrating along the entire coastline (five sectors), the shoreline eroded by 50.4 m on averaged (0.6 m/yr), with large multi-decadal variability (Fig. 6c).

4.2. Bathymetric evolution since 1903

Fig. 9 shows the shallow water bathymetric evolution from 1903 to 2021 of the southern pass of the Gironde estuary mouth, offshore of the North-Médoc coastline. It highlights the large morphological variability over the past 118 years. Since 1903, the sand volume in the computation box (Fig. 9a) has decreased (−20.16 millions of m^3 within 20,125 km^2, Fig. 9g,h). The delimitation of the rocky substratum discriminates two sandy shoals from the shallow rocky area. The first shoal (bubble 1 in Fig. 9a), which dynamics is shown in more detail in Fig. 10, was located approximately 1 km offshore, south of Soulac-sur-Mer in 1909, Sector (2) (Figs. 9a and 10a). This shoal progressively migrated onshore. Between 1909 and 1929, it welded to the coast within Sector (2) (Figs. 9b and 10b) and stretched along the coastline during the subsequent years (Fig. 10c). From 1909 to 2021 within 2020 km^2 (Fig. 10d), approximately 4.5 million m^3 of sand have been lost offshore of the accreting shoreline sectors (Fig. 2), indicating that the shoal mostly fed the sandy beaches.

In 1909, a second shoal (bubble 2, in Sector (3), in Fig. 9a) can be identified further northeast (Figs. 9a and 11a). This mostly alongshore oriented shoal increased in size (Fig. 11b) and volume, as approximately 1.8 million m^3 were gained (Fig. 11d) between 1909 and 1935. During this time interval, the second shoal was connected to the first shoal (e.g. 1935, Fig. 11b, marked by the black star) and smaller shoals bypassed the *South Pass* (Fig. 9b, event marked by the red star) and welded to the alongshore shoal (identified from the 18 high-frequency bathymetric maps from 1903 to 1939, not shown). After 1935, sand volume tended to decrease at an unsteady rate. The shoal gradually migrated towards the northeast (Cape Grave) apparently supplying Sector (5) with a large amount of sediment. Its volume and size reduced over the years (−5.33 millions of m^3 within a 3785 km^2 area, Fig. 11d) until it almost disappeared in the most recent bathymetric map (i.e. 2021, Fig. 11c).

The third remarkable feature in the shallow water bathymetry

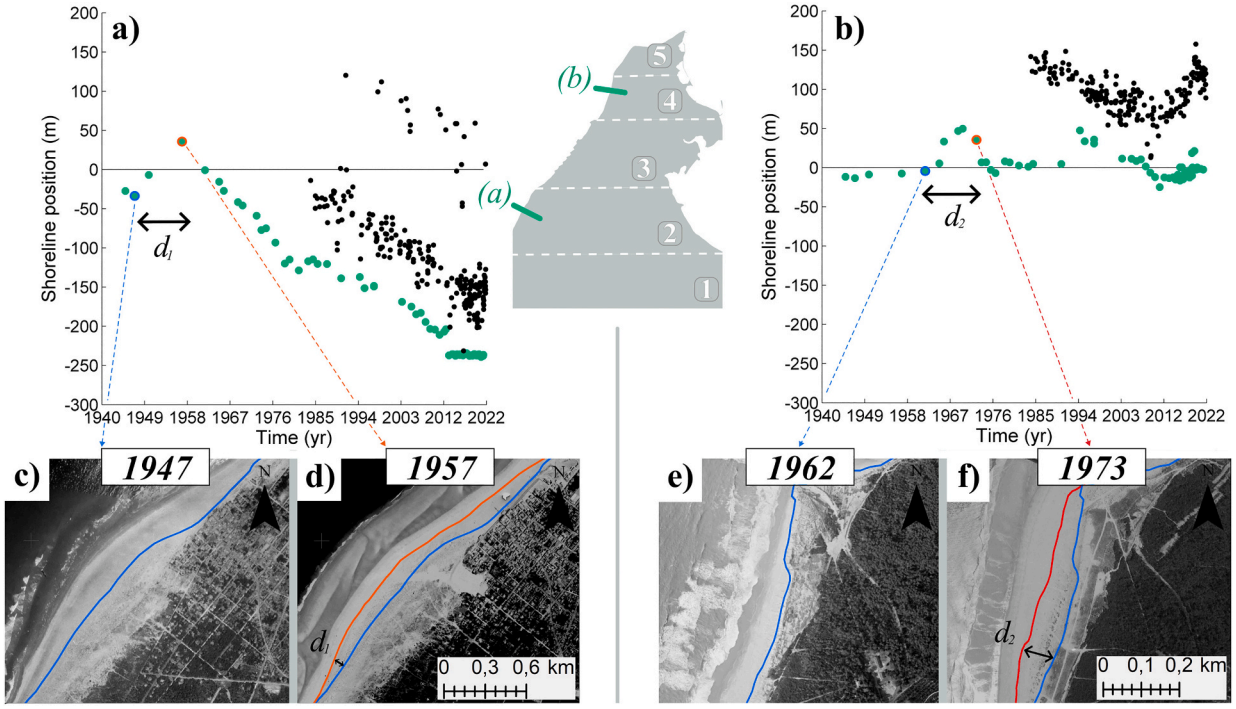

Fig. 7. Temporal changes in the shoreline position at transects (a) and (b), which are situated on the gray map, demonstrate periods of accretion (and distance) (*d1*) from (c) 1947 to (d) 1957 at Soulac-sur-Mer, sector (2), and (*d2*) from (e) 1962 to (f) 1973, at sector (4). Dune foot shoreline and satellite-derived waterline are shown in green and black, respectively, see Table 1. (For interpretation of the references to colour in this figure legend, the reader is referred to the web version of this article.)

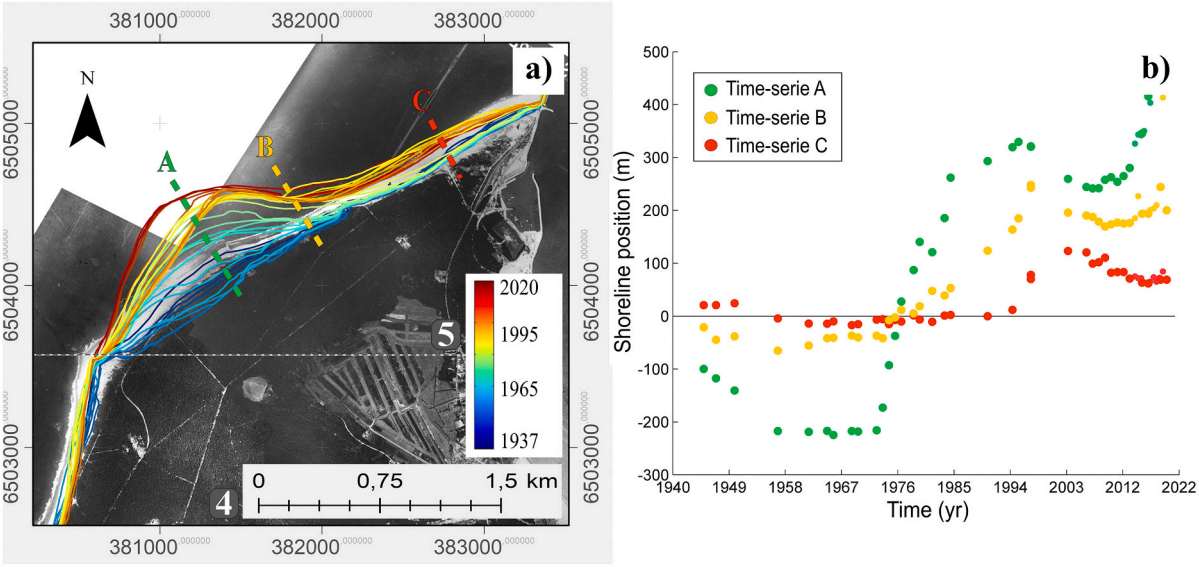

Fig. 8. Evolution of shoreline position between 1937 and 2020 at Sector (5), in the north of the study site: (a) orthophotograph of 1937 with superimposed shorelines (date coloured) with the three dotted lines (green, yellow and red) indicating the locations at which shoreline position time series are extracted in (b). (For interpretation of the references to colour in this figure legend, the reader is referred to the web version of this article.)

evolution is the formation of a channel that opened approximately 1 km off Cape Négade, at Sector (1), ($x = 1.5$ km, Fig. 1e) since 1959, between the rocky shoal and the coastline (Fig. 9c and 12a). In this area which appears relatively stable during the first part of the 20th century, the channel gradually deepened (widened) during the second part of the 20th century, until it reached a depth (width) of −9 m to −10 m IGN/NGF69 (700 m). The link between this channel and the continuous shoreline erosion along those sectors, (1) and (2), will be discussed later in this paper.

5. Discussion

5.1. Conceptual model

We show that the North-Médoc coast has been chronically eroding over the last century at a mean rate of 0.6 m/yr. This is in line with the chronic erosion observed along this coastline by Lévèque (1936); Allen et al. (1974b); Howa (1987) from the 1700s to the early 1900s, and even earlier since ca. 3500 BP (Stéphan et al., 2019). However, while erosion

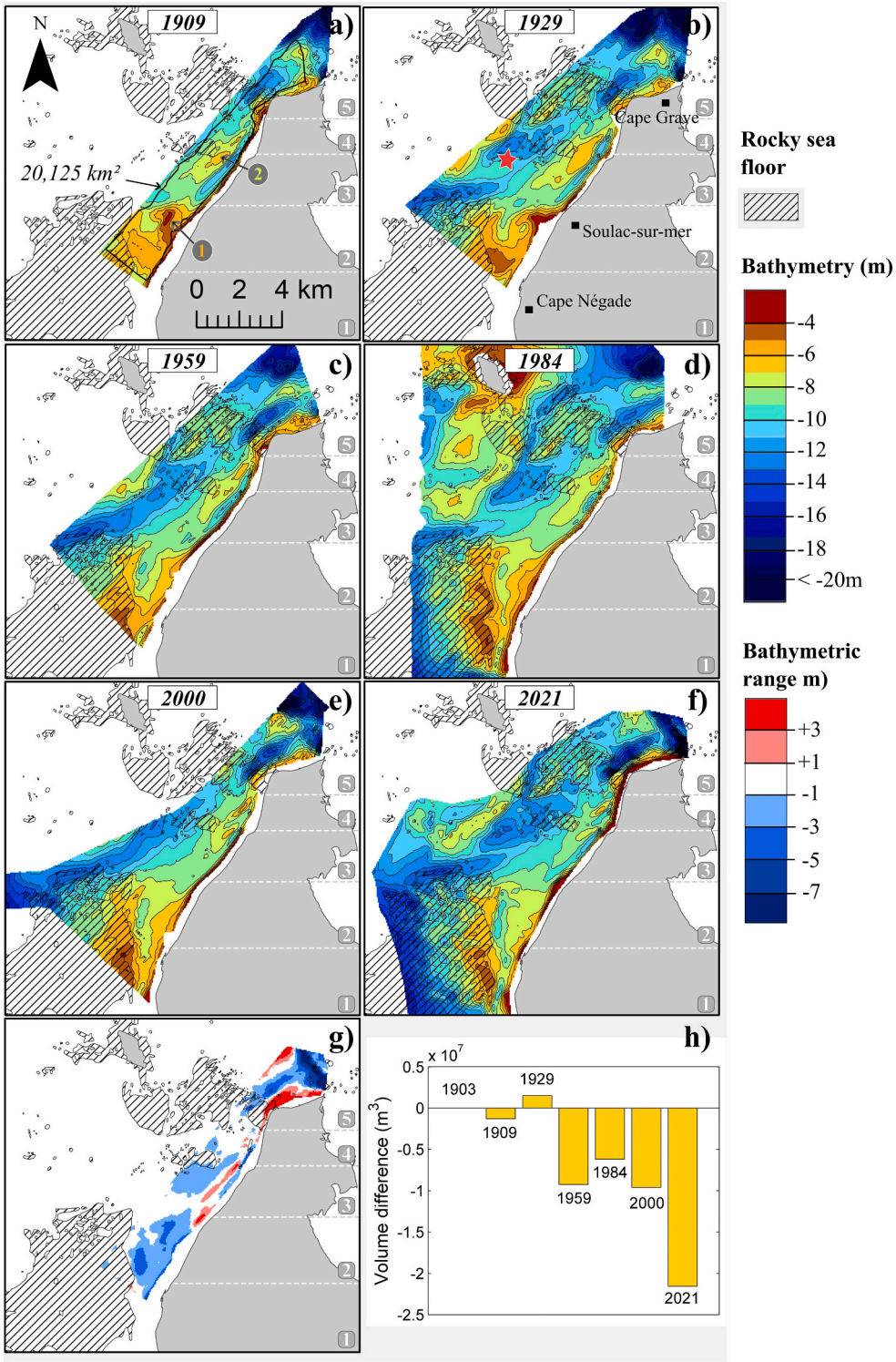

Fig. 9. (a-f) Shallow water bathymetric evolution (IGN/NGF69) from 1909 to 2021 using a selection of the dataset listed in Table 2, (g) difference plot between 1909 and 2021 and (h) time series of the volume change since 1903 in the computation box shown in (a). The red star shows the location where smaller shoals by-passed the South Pass.

rates were previously observed to increase northwards (e.g. Howa, 1987), the more recent changes documented herein show chronic erosion rates decreasing northwards, with even locally accreting sectors at the northern end of the study site (Fig. 6b). Interestingly enough, the alongshore-average chronic erosion rate of 0.6 m/yr is on the same order of the erosion rate averaged across the entire southwest coast of France (Castelle et al., 2018), despite the coastline studied herein is iconic of coastal erosion for metropolitan France. This is because the most erosive sectors of our study site are primarily located in the urbanized areas (Fig. 6b). Contrary to previous work on longer timescales which suggested a monotonic erosion over the entire domain (Lévêque, 1936; Allen et al., 1974b; Howa, 1987), our work based on historical charts and multiple sources of topo-bathymetric data suggests much more complex behaviour over time and space. The time series of alongshore-

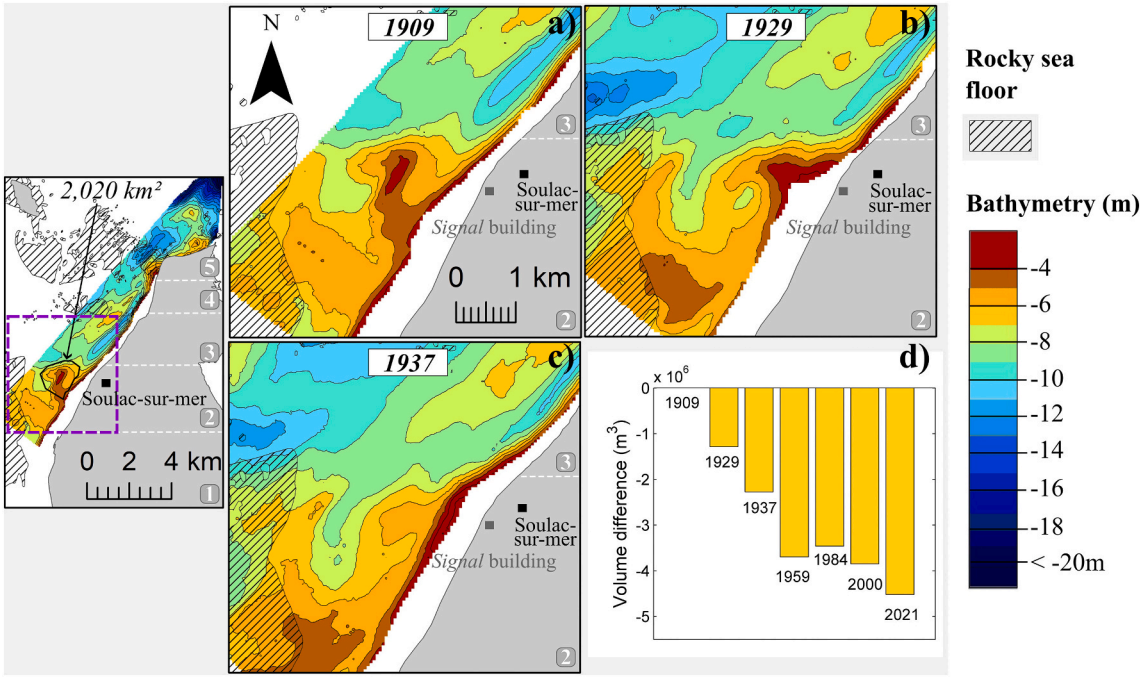

Fig. 10. Shallow water bathymetric evolution (IGN/NGF69) of (a) the shoal located 1 km offshore of Soulac-sur-Mer in 1909 and (b) in 1929 and (c) 1937, welding to the coast, with (d) the time series of the volume change since 1909 in the computation box shown in left-hand panel.

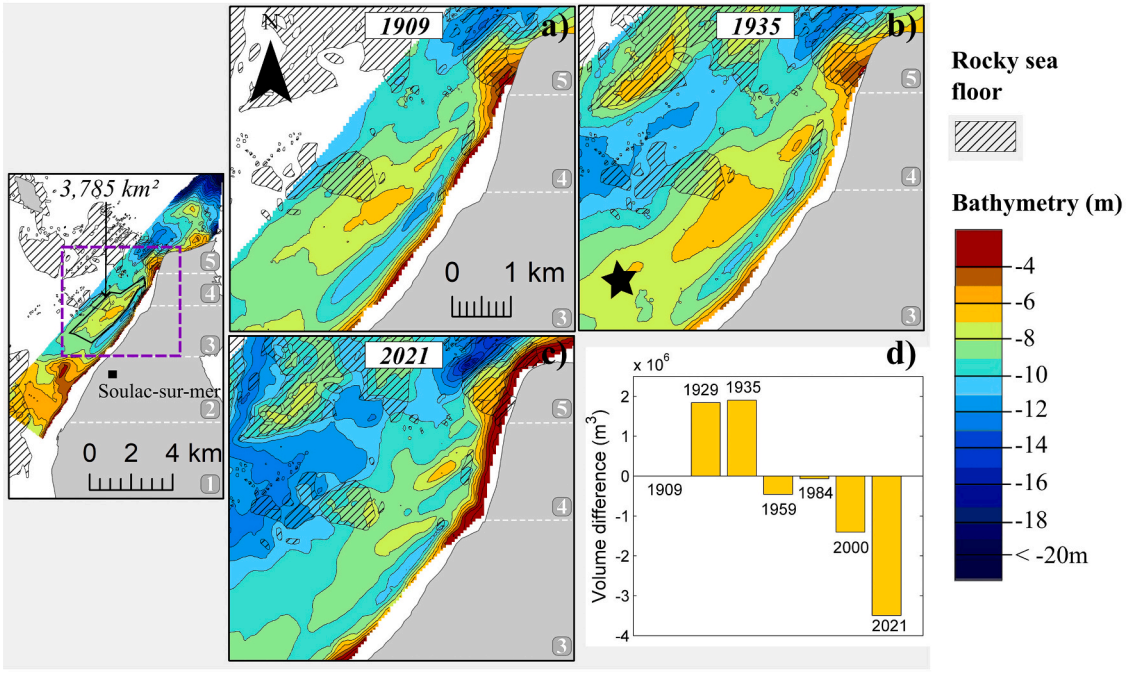

Fig. 11. Shallow water bathymetric evolution (IGN/NGF69) of the alongshore-oriented shoal (a) in 1909, b) in 1929 and (c) in 2021 with (d) the time series of the volume change since 1909 in the computation box shown in left-hand panel. The black star shows the connection between the first shoal (outside the frame) and the alongshore-oriented shoal.

averaged shoreline position shown in Fig. 6c can be viewed as the superimposition of the large-scale accretion event in sector (5) onto a quasi-steady long-term erosive trend (Fig. 6b) primarily across the first and second sectors. Such large shoreline variability if often found close to tidal inlet or estuary mouth (Hansen et al., 2013; Velasquez-Montoya et al., 2020; Castelle et al., 2021) and linked with shoal attachment to the downdrift coast (FitzGerald, 1982, 1984; Ridderinkhof et al., 2016a; Burvingt et al., 2022). In line with these observations globally, our results indicate that shoreline change observed along the entire sector (Section 4.1) is largely enforced by such bathymetric changes (Section 4.2), with two major shoal welding events (in the 1920s and 1950s). Such dynamics is also largely influenced by rocky platform and outcrops. Our results are synthesised in a conceptual model proposed in Fig. 13, which is further discussed below.

The first shoal progressively attached to the south of Soulac-sur-Mer between 1903 and 1929 (Sector (2), Fig. 10). Despite the absence of

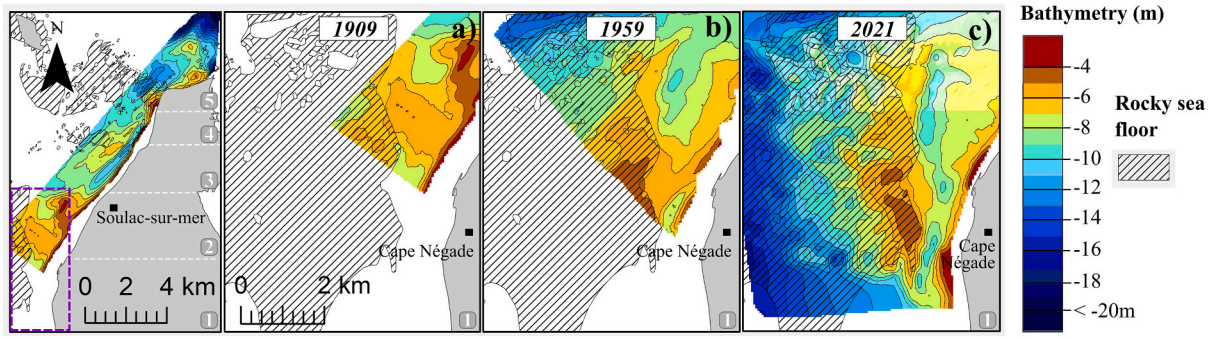

Fig. 12. Shallow water bathymetric evolution (IGN/NGF69) of the alongshore channel offshore of Cape Négade which was (a) absent in 1909 (b) developed in the mid-20th century before (c) becoming an alongshore channel.

shoreline data at that time, we hypothesize that such attachment drove a large, localized, shoreline accretion (Fig. 13a). This nearly 4.5 million m^3 sand supply was sustained until approximately the 1920s (Fig. 13b). It is evidenced by the large, 350-m wide, bare sand beach facing the Signal building (see Fig. 13b, sector (2)). The absence of vegetation on the 1937 orthomosaic (not shown) testifies the recentness of the shoreline bulge. According to bathymetric and shoreline data, the shoreline bulge diffused and migrated predominantly (downdrift) northeastwards (see shoreline accretion in the bottom panels of Fig. 7a), until the late 1950s (Fig. 13c). This process contributed in feeding the beach of Soulac-sur-Mer as shown in the large beach accretion observed in Fig. 2b. Until the 1980s (Fig. 13d) continuous erosion of the southern beaches was observed. This erosion was attributed to the lack of offshore sand supply, as evidenced by the conversion of a 350-m wide bare sand bulge to a 200-m wide, vegetated, dune in front of the Signal Building (photograph of 1970s in Fig. 3b). In contrast, the second shoal is hypothesized to feed Sector (5) since the 1950s, first stopping shoreline erosion in Sector (5) in the 1950s and subsequently driving dramatic localized accretion in the 1970s (Figs. 8 and 13d). This behaviour continued over the last decades (Fig. 13e), as both chronic erosion along the southern coast and accretion in the northern sector continued. This accretion was caused by the second shoal intermittently benefiting from offshore sediment supply (using a detailed inspection of all the available bathymetric data, not shown). In contrast, the alongshore channel which has been progressively deepening south of Soulac-sur-Mer since nearly the 1970s (Fig. 12c) is hypothesized to further limit sediment supply to the southern beaches.

The long-time chronically eroding North-Médoc coast has experienced two recent bursts of sediment supply from shoal attachment, which are typically driven by ebb delta dynamics (e.g. Lenstra et al., 2019; Burvingt et al., 2022). However, along the most urbanized area (Sectors (1) to (3), Fig. 6a and Fig. 9f) the system has shifted from a sediment-rich to a sediment poor environment in the early 19th century, leading to continued shoreline erosion and the absence of subsequent shoal attachments along this sector. The material presented herein cannot help determining why sediment supply from the offshore area has stopped, which would require long-term (> 100 years) large-scale (entire estuary mouth) bathymetric data. Amongst the hypotheses that should be explored is the potential influence of sea level rise, driving increased tidal prism (Fitzgerald et al., 2004) and tidal currents (O'Brien, 1931, 1969; FitzGerald et al., 2008), which in turn can affect channel morphology (e.g. Nahon et al., 2019) and sediment dynamics (Van Goor et al., 2003). In addition, the main Gironde estuary channel further north (*West Pass*, Fig. 1a) experienced major dredging operations in the early 1930s (Lévêque, 1936), and regular aggregate extraction operations have been performed, which effects may have cascaded downdrift and limited sediment availability offshore of our study site. The combined effects of sea level rise and major dredging and aggregate extraction operations may have thus affected the large-scale behaviour of the Gironde estuary mouth, as evidenced elsewhere by the impact of increasing tidal prism (Fitzgerald et al., 2004) or channels deepening (FitzGerald et al., 2008) on ebb tidal delta morphology (O'Brien, 1931, 1969; Van Goor et al., 2003). Such changes can result in a decrease in drifting shoals from the ebb tidal delta to the adjacent coast, or alongshore channel deepening (Fig. 12c), resulting in reduced sediment supply (Gaudiano and Kana, 2001; Ridderinkhof et al., 2016a) and coastal erosion. Addressing this issue is out of scope and would require additional, large-scale and long-term, bathymetric datasets as well as detailed process-based numerical modelling.

5.2. *Implications for coastal management*

As indicated in Section 2, a large number of groynes and seawalls have been progressively erected over the two last centuries, with the primary objective to protect erosion-threatened infrastructures (Pilkey and Wright, 1988; Basco, 2006; Neshaei and Biria, 2013) but also formerly to prevent the breaching of the coast at Sector (3). Although the beaches further south continued to erode, most of these coastal interventions successfully stabilized the shoreline locally, occasionally leading to localized beach loss. However, these measures did not significantly affect the overall evolution of the shoreline at the adjacent sectors. A notable exception is the groyne delimiting Sectors (2) and (3), located north of Soulac-sur-Mer, which was repaired and further extended in 2014 and successfully traps sediments from the dominant northerly longshore drift. Since 2014, the beach in front of Soulac-sur-Mer has been progressively widening and has been used since 2019 as the main source of sediment to nourish each spring the most eroding beaches further south. Such regular beach nourishments (around 60.10^3 m^3/yr each spring since 2019), but also other non-documented irregular nourishments performed in the early 2000s further south, can buffer storm waves during low-energy winters (Hamm et al., 2002). However, they are not viewed as a long-term approach as shoreline erosion is sustained. On the other hand, mega-nourishments (20 million m^3 in the case of the Sand Engine, Stive et al., 2013) can be viewed as an appealing alternative. Such approach, however, needs to be designed carefully (e.g. Mulder and Tonnon, 2011; de Schipper et al., 2014, 2016; Luijendijk et al., 2017). In this frame, the first shoal welding completed in the 1920s, with an approximately 5 million m^3 sediment input, can provide preliminary valuable information on the fate of a mega-nourishment, which could be located in the same location of the observed natural shoal attachment ($x = 4$ km, Fig. 13). The absence of shoreline data prior to the shoal attachment prevents from accurately computing such beach nourishment lifetime. However, given the steady erosion rate of the order of 5 m/year in the alignment of the nearly 5 million m^3 shoal attachment resulting in a practically 350-m wide beach in its centre, a first-pass estimate of the nourishment lifetime would be approximately 70 years. However, we hypothesize that it is a strong overestimation as the current bathymetric configuration is less optimistic than in the early 1900s. The absence of shoals offshore and the continuous deepening of the alongshore channel (Fig. 12c) should largely increase the diffusion

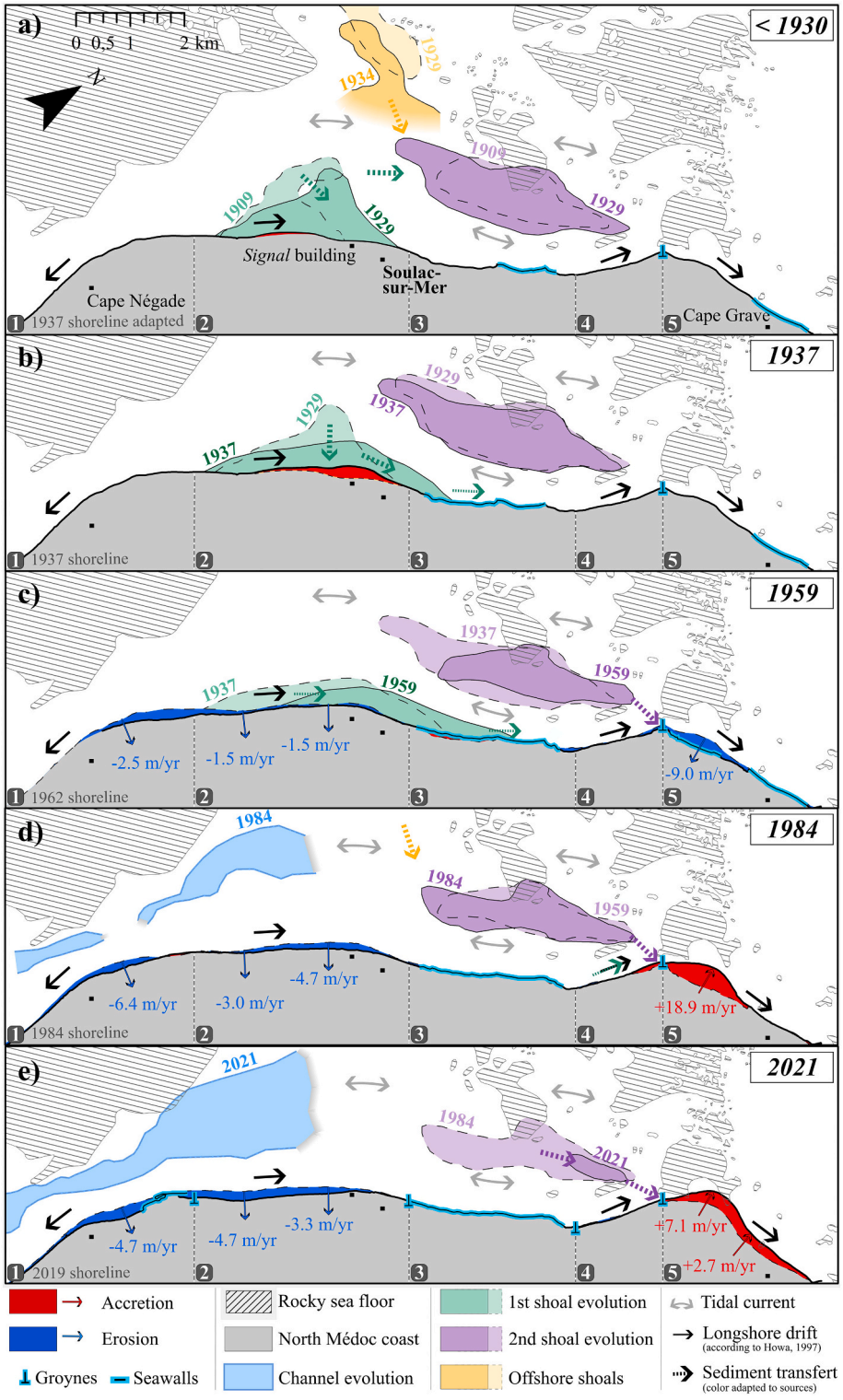

Fig. 13. Conceptual model of the study site from the beginning of the 20th century. (a) Before 1930: shoal #1 (green) offshore of sector (2) migrating and welding to the coast within 20 years; (b) diffusion of the shoreline bulge with slow downdrift migration, reaching Sector (3). (c) After 1959, the northward progression of Shoal #1 is no longer apparent, although it hypothesized to supply Sector (5) with sediment. (a) Prior 1930: shoal #2 (purple) offshore of Sector (3) expanded, benefiting from offshore sediment supply (yellow), (c) migrated towards Sector (5) and drove shoreline accretion (d,e). (d) Since 1984, a channel appears between the coast (gray) and the rocky sea floor (gray stripes), (e) further deepening and widening. The *Signal building* position is given for reference in each panel. Primary location names are provided in (a). (For interpretation of the references to colour in this figure legend, the reader is referred to the web version of this article.)

rate of a mega-nourishment. In addition, a mega-nourishment at the exact same location would not counteract coastal erosion further south, at Sector (2), but mostly in the area facing the Signal building. A mega-nourishment extending further alongshore southwards should protect a longer coastal sector, but would dramatically reduce its lifetime.

A detailed morphodynamic modelling study, combining process-based (e.g. Luijendijk et al., 2017) and reduced-complexity (e.g. Robinet et al., 2018) models should be performed in order to provide more robust and quantitative insight into the optimal design and expected lifetime of such mega-nourishments. Process-based models implemented on the Gironde estuary (e.g. Jalón-Rojas et al., 2015; Huybrechts et al., 2021) should consider the action of breaking waves and non-cohesive sediment transport to better identify sediment pathways. Using past and current bathymetric configurations, the differences in sediment pathways and potential for shoal welding to the coast could be explored. Such process-based models could also be used to address the impact of sea level rise and dredging operations on the cascading long-term changes of the estuary mouth and adjacent coasts. However, it must be stressed that the process-based modelling of such complex (multiple shoal and channel systems, rocky substratum, …), large-scale, estuary mouth exposed to high-energy waves and co-existing non-cohesive and cohesive sediment processes is challenging, especially with the lack of field data covering the entire system. Reduced-complexity shoreline models (e.g. Vitousek et al., 2017; Antolínez et al., 2019; Robinet et al., 2018) can be powerful tools to hindcast and forecast shoreline change on long timescales with relatively cheap computational cost. Such models have been successfully used to hindcast the multi-year evolution of the Sand Engine and to provide estimations of the mega-nourishment lifetime (e.g. Arriaga et al., 2017; Roelvink et al., 2020). Such approach assumes, however, an alongshore-uniform and time invariant shoreface and the absence of e.g. deepening alongshore channels and ebb tidal data. We advocate that combining process-based and reduced complexity models is a relevant approach to further improve our understanding of shoreline change and the evolution of a potential mega-nourishment along the North-Médoc coast.

6. Conclusions

Since at least the early 20th century, the North-Médoc coast sector, southwest France, which is adjacent to the largest estuary in Europe, has been exposed to extreme erosion threatening coastal infrastructures. By combining 84 years of shoreline data from various sources, 118 years of shallow water bathymetric surveys and historical photographs, the spatial and temporal patterns of shoreline change were quantitatively described, and their primary driver were unravelled. We show that shoreline change is essentially enforced by bathymetric changes and shoal attachments. In contrast, smallscale beach nourishments and coastal works (groynes, seawall) only temporally buffer erosion or lastingly locally fix the shoreline, respectively. Two major shoal attachments to the shore were identified. Although with different timing, magnitude and location these shoal attachment events dominate the past temporal and spatial shoreline variability. Of particular importance was the shoal attachment occurring in the 1920s south of Soulac-sur-Mer. While it locally largely widened and rose the beaches, during the subsequent decades a progressive diffusion of this sediment-starved shoreline bulge was observed, resulting in a quasi-steady erosion peaking at approximately 5.4 m/year. In contrast, the second shoal attachment drove dramatic shoreline accretion locally in a remote sector of the coast, with sustained sediment supply allowing continued shoreline accretion. The first shoal attachment provides a unique natural analogue for a potential mega-nourishment of the most eroding sector of the coast, which is currently viewed as the only sustainable soft solution to limit coastal erosion. We anticipate that this study, together with future modelling work, will help the coastal managers and decision makers to better design their future coastal management strategy.

Declaration of competing interest

The authors declare that they have no known competing financial interests or personal relationships that could have appeared to influence the work reported in this paper.

Data availability

Data will be made available on request.

Acknowledgements

This work is part of the project ESTOC, co-funded by the Region Nouvelle-Aquitaine, the Communauté de Communes Médoc Atlantique (CCMA), the BRGM and EPOC (University of Bordeaux - CNRS). BC received funding from Agence Nationale de la Recherche (ANR) grant number ANR-21-CE01-0015 (SHORMOSAT). The authors would like to thank the Grand Port Maritime de Bordeaux (GPMB) for kindly providing access to their archives and to historical nautical charts, the Observatoire de la Côte Nouvelle Aquitaine (OCNA) for historic shoreline data as well as the Institut Géographique National (IGN) for open access aerial photographs. We would also like to thank Kilian Vos and the Water Research Laboratory for developing and making freely available the CoastSat toolkit.

References

Allen, G.P., 1991. Sedimentary Processes and Facies in the Gironde Estuary: A Recent Model for Macrotidal Estuarine Systems.

Allen, G.P., Bonnefille, R., Courtois, G., Migniot, C., 1974a. Processus de sédimentation des vases dans l'estuaire de la Gironde Contribution d'un traceur radioactif pour l'étude du déplacement des vases. La Houille Blanche 60, 129–136. https://doi.org/10.1051/lhb/1974013.

Allen, G.P., Bouchet, J.-M., Carbonel, P., Castaing, P., Gayet, J., Gonthier, E., Jouanneau, J.-M., Klingebiel, A., Latouche, C., Legigan, P., Orgeron, C., Pujos, M., Tesson, M., Vernette, G., 1974b. Environnements et processus sédimentaires sur le littoral Nord-Aquitain. Bull. Inst. géol. Bassin Aquitaine.

Antolínez, J.A.A., Mendez, F.J., Anderson, D., Ruggiero, P., Kaminsky, G.M., 2019. Predicting climate-driven coastlines with a simple and efficient multiscale model. J. Geophys. Res. Earth 124, 1596–1624. https://doi.org/10.1029/2018JF004790.

Arriaga, J., Rutten, J., Ribas, F., Falques, A., Ruessink, G., 2017. Modeling the long-term diffusion and feeding capability of a mega-nourishment. Coast. Eng. 121, 1–13. https://doi.org/10.1016/j.coastaleng.2016.11.011.

Bamunawala, J., Ranasinghe, R., Dastgheib, A., Nicholls, R.J., Murray, A.B., Barnard, P. L., Sirisena, T., Duong, T.M., Hulscher, S.J.M.H., van der Spek, A., 2021. Twenty-first-century projections of shore- line change along inlet-interrupted coastlines. Sci. Rep. 11 https://doi.org/10.1038/s41598-021-93221-9.

Basco, D.R., 2006. Seawall impacts on adjacent beaches: separating fact from fiction. J. Coast. Res. 441–744.

Burvingt, O., Lerma, A.N., Lubac, B., Mallet, C., Senechal, N., 2022. Geomorphological control of sandy beaches by a mixed-energy tidal inlet. Mar. Geol. 450, 106863 https://doi.org/10.1016/j.margeo.2022.106863.

Byrne, R., Gammisch, R., Thomas, G., 1980. Tidal Prism-Inlet Area Relations for Small Tidal Inlets, pp. 2517–2533. https://doi.org/10.1061/9780872622647.151.

Castaing, P., Allen, G.P., 1981. Mechanisms controlling seaward escape of suspended sediment from the Gironde: a macrotidal estuary in France. Mar. Geol. 40, 101–118. https://doi.org/10.1016/0025-3227(81)90045-1.

Castelle, B., Masselink, G., 2023. Morphodynamics of wave-dominated beaches. Cambridge Prisms: Coastal Futures 1, e1. https://doi.org/10.1017/cft.2022.2.

Castelle, B., Marieu, V., Bujan, S., Splinter, K.D., Robinet, A., Sénéchal, N., Ferreira, S., 2015. Impact of the winter 2013–2014 series of severe Western Europe storms on a double-barred sandy coast: beach and dune erosion and megacusp embayments. Geomorphology 238, 135–148. https://doi.org/10.1016/j.geomorph.2015.03.006.

Castelle, B., Bujan, S., Ferreira, S., Dodet, G., 2017. Foredune morphological changes and beach recovery from the extreme 2013/2014 winter at a high-energy sandy coast. Mar. Geol. 385, 41–55. https://doi.org/10.1016/j.margeo.2016.12.006.

Castelle, B., Guillot, B., Marieu, V., Chaumillon, E., Hanquiez, V., Bujan, S., Poppeschi, C., 2018. Spatial and temporal patterns of shoreline change of a 280-km high-energy disrupted sandy coast from 1950 to 2014: SW France. Estuar. Coast. Shelf Sci. 200, 212–223. https://doi.org/10.1016/j.ecss.2017.11.005.

Castelle, B., Masselink, G., Scott, T., Stokes, C., Konstantinou, A., Marieu, V., Bujan, S., 2021. Satellite-derived shoreline detection at a high-energy meso-macrotidal beach. Geomorphology 383, 107707. https://doi.org/10.1016/j.geomorph.2021.107707.

Castelle, B., Ritz, A., Marieu, V., Nicolae Lerma, A., Vandenhove, M., 2022. Primary drivers of multidecadal spatial and temporal patterns of shoreline change derived from optical satellite imagery. Geomorphology 413, 108360. https://doi.org/10.1016/j.geomorph.2022.108360.

CDCMA, 2021a. Analyse de l'évolution récente (2013-2021) du littoral de la pointe de la Négade (Soulac-sur-Mer) à la jetée de Grave (Verdon-sur-Mer). Technical Report. Casagec Engineering.
CDCMA, 2021b. Rapport de levé bathymétrique, suivi bathymétrique Médoc: de la pointe de la Négade à la jetée de Grave. Technical Report. Seaviews.
de Schipper, M.A., De Vries, S., Stive, M., De Zeeuw, R., Rutten, J., Ruessink, G., Aarninkhof, S., Van Gelder-Maas, C., 2014. Morphological development of a mega-nourishment; first observations at the Sand Engine. Int. Conf. Coastal Eng. 1, 73. https://doi.org/10.9753/icce.v34.sediment.73.
de Schipper, M.A., de Vries, S., Ruessink, G., de Zeeuw, R.C., Rutten, J., van Gelder-Maas, C., Stive, M.J., 2016. Initial spreading of a mega feeder nourishment: Observations of the Sand Engine pilot project. Coast. Eng. 111, 23–38. https://doi.org/10.1016/j.coastaleng.2015.10.011.
de Schipper, M.A., Ludka, B.C., Raubenheimer, B., Luijendijk, A.P., Schlacher, T.A., 2021. Beach nourishment has complex implications for the future of sandy shores. Nat. Rev. Earth Environ 2, 70–84. https://doi.org/10.1038/s43017-020-00109-9.
De Swart, H., Zimmerman, J., 2009. Morphodynamics of tidal inlet systems. Annu. Rev. Fluid Mech. 41, 203–229. https://doi.org/10.1146/annurev.fluid.010908.165159.
Dundon, L.A., Abkowitz, M., 2021. Climate-induced managed retreat in the U.S.: a review of current research. Climate. Risk Manage. 33, 100337 https://doi.org/10.1016/j.crm.2021.100337.
Elias, E.P., Van der Spek, A.J., Pearson, S.G., Cleveringa, J., 2019. Understanding sediment bypassing processes through analysis of high-frequency observations of ameland inlet, the Netherlands. Mar. Geol. 415, 105956 https://doi.org/10.1016/j.margeo.2019.06.001.
Ells, K., Murray, A.B., 2012. Long-term, non-local coastline responses to local shoreline stabilization. Geophys. Res. Lett. 39 https://doi.org/10.1029/2012GL052627.
FitzGerald, D.M., 1982. Sediment Bypassing at Mixed Energy Tidal Inlets, pp. 1094–1118. https://doi.org/10.1061/9780872623736.068.
FitzGerald, D.M., 1984. Interactions between the Ebb-Tidal Delta and Landward shoreline: Price Inlet, South Carolina. SEPM JSR 54. https://doi.org/10.1306/212F85C6-2B24-11D7-8648000102C1865D.
Fitzgerald, D.M., Kulp, M., Penland, S., Flocks, J., Kindinger, J., 2004. Morphologic and stratigraphic evolution of muddy ebb-tidal deltas along a subsiding coast: Barataria Bay, Mississippi River delta. Sedimentology 51, 1157–1178. https://doi.org/10.1111/j.1365-3091.2004.00663.x.
FitzGerald, D.M., Fenster, M.S., Argow, B.A., Buynevich, I.V., 2008. Coastal Impacts due to sea-level rise. Annu. Rev. Earth Planet. Sci. 36, 601–647. https://doi.org/10.1146/annurev.earth.35.031306.140139.
Fortunato, A.B., Nahon, A., Dodet, G., Rita Pires, A., Conceicao Freitas, M., Bruneau, N., Azevedo, A., Bertin, X., Benevides, P., Andrade, C., Oliveira, A., 2014. Morphological evolution of an ephemeral tidal inlet from opening to closure: the Albufeira inlet, Portugal. Cont. Shelf Res. 73, 49–63. https://doi.org/10.1016/j.csr.2013.11.005.
Gaudiano, D., Kana, T., 2001. Shoal bypassing in mixed energy inlets: geomorphic variables and empirical predictions for nine South Carolina inlets. J. Coast. Res. 17, 280–291.
Hamm, L., Capobianco, M., Dette, H., Lechuga, A., Spanhoff, R., Stive, M., 2002. A summary of European experience with shore nourishment. Coast. Eng. 47, 237–264. https://doi.org/10.1016/S0378-3839(02)00127-8.
Hansen, J.E., Elias, E., List, J.H., Erikson, L.H., Barnard, P.L., 2013. Tidally influenced alongshore circulation at an inlet-adjacent shoreline. Cont. Shelf Res. 56, 26–38. https://doi.org/10.1016/j.csr.2013.01.017.
Harley, M.D., Turner, I.L., Kinsela, M.A., Middleton, J.H., Mumford, P.J., Splinter, K.D., Phillips, M.S., Simmons, J.A., Hanslow, D.J., Short, A.D., 2017. Extreme coastal erosion enhanced by anomalous extratropical storm wave direction. Sci. Rep. 7 https://doi.org/10.1038/s41598-017-05792-1.
Hayes, M.O., Goldsmith, V., Hobbs, C.H., 1970. Offset coastal inlets. Coast. Eng. Proc. 1, 75. https://doi.org/10.9753/icce.v12.75.
Hine, A.C., 1979. Mechanisms of berm development and resulting beach growth along a barrier spit complex. Sedimentology 26, 333–351. https://doi.org/10.1111/j.1365-3091.1979.tb00913.x.
Howa, H., 1987. Le littoral du Nord Medoc, (Gironde) - Evolution d'une cote sableuse en erosion. Thesis University or Bordeaux I. Soc. Geol. France, p. 258.
Howa, H., 1997. Sediment budget in the southern inlet of the Gironde Estuary (SW France). Phys. Chem. Earth 22, 373–375. https://doi.org/10.1016/S0079-1946(97)00160-2.
Huybrechts, N., Smaoui, H., Orseau, S., Tassi, P., Klein, F., 2021. Automatic calibration of bed friction coefficients to reduce the influence of seasonal variation: case of the Gironde Estuary. J. Waterw. Port Coast. Ocean Eng. 147, 05021004. https://doi.org/10.1061/(ASCE)WW.1943-5460.0000632.
Idier, D., Castelle, B., Charles, E., Mallet, C., 2013. Longshore sediment flux hindcast: spatio-temporal variability along the SW Atlantic coast of France. J. Coast. Res. 165, 1785–1790. https://doi.org/10.2112/SI65-302.1.
Jalón-Rojas, I., Schmidt, S., Sottolichio, A., 2015. Turbidity in the fluvial Gironde Estuary (southwest France) based on 10-year continuous monitoring: sensitivity to hydrological conditions. Hydrol. Earth Syst. Sci. 19, 2805–2819. https://doi.org/10.5194/hess-19-2805-2015.
Jouanneau, J., Weber, O., Cremer, M., Castaing, P., 1999. Fine-grained sediment budget on the continental margin of the Bay of Biscay. Deep-Sea Res. II Top. Stud. Oceanogr. 46, 2205–2220. https://doi.org/10.1016/S0967-0645(99)00060-0.
Konstantinou, A., Scott, T., Masselink, G., Stokes, K., Conley, D., Castelle, B., 2023. Satellite-based shoreline detection along high-energy macrotidal coasts and influence of beach state. Mar. Geol. 462, 107082 https://doi.org/10.1016/j.margeo.2023.107082.
Lafon, V., Hoareau, A., Mallet, C., Desprat, F.F., 2010. Suivi du trait de côte en aquitaine par imagerie formosat-2. In: The Proceedings of XIèmes Journées Nationales Génie Côtier – Génie Civil, Paralia. https://doi.org/10.5150/jngcgc.2010.058-L.
Laporte-Fauret, Q., Castelle, B., Marieu, V., Nicolae-Lerma, A., Rosebery, D., 2022. Foredune blowout formation and subsequent evolution along a chronically eroding high-energy coast. Geomorphology 414, 108398. https://doi.org/10.1016/j.geomorph.2022.108398.
Lenstra, K.J.H., Pluis, S.R.P.M., Ridderinkhof, W., Ruessink, G., van der Vegt, M., 2019. Cyclic channel-shoal dynamics at the Ameland inlet: the impact on waves, tides, and sediment transport. Ocean Dyn. 69, 409–425. https://doi.org/10.1007/s10236-019-01249-3.
Lévêque, F., 1936. Bordeaux et l'estuaire girondin: Amélioration des acccès maritimes du port de Bordeaux, Imprimeries delmas de. Bordeaux.
Lubac, B., Burvingt, O., Nicolae Lerma, A., Sénéchal, N., 2022. Performance and uncertainty of satellite-derived bathymetry empirical approaches in an energetic coastal environment. Remote Sens. 14 https://doi.org/10.3390/rs14102350.
Luijendijk, A.P., Ranasinghe, R., de Schipper, M.A., Huisman, B.A., Swinkels, C.M., Walstra, D.J., Stive, M.J., 2017. The initial morphological response of the Sand Engine: a process-based modelling study. Coast. Eng. 119, 1–14. https://doi.org/10.1016/j.coastaleng.2016.09.005.
Luijendijk, A.P., Hagenaars, G., Ranasinghe, R., Baart, F., Donchyts, G., Aarninkhof, S.G.J., 2018. The state of the world's beaches. Sci. Rep. 8, 1–11. https://doi.org/10.1038/s41 598-018-24630-6.
Mallet, C., Howa, H., Garlan, T., Sottolichio, A., Le Hir, P., Michel, D., 2000. Utilisation of numerical and statistical techniques to describe sedimentary circulation patterns in the mouth of the Gironde estuary. C. R. Acad. Sci. Ser. II 331, 491–497. https://doi.org/10.1016/S1251-8050(00)01437-3.
Masselink, G., Castelle, B., Scott, T., Dodet, G., Suanez, S., Jackson, D., Floc'h, F., 2016. Extreme wave activity during 2013/2014 winter and morphological impacts along the Atlantic coast of europe. Geophys. Res. Lett. 43, 2135–2143. https://doi.org/10.1002/2015GL067492.
Mulder, J.P., Tonnon, P.K., 2011. "Sand Engine": background and design of a mega-nourishment pilot in the Netherlands. Int. Conf. Coastal Eng. 1, 35. https://doi.org/10.9753/icce.v32.management.35.
Nahon, A., Idier, D., Sénéchal, N., Féniès, H., Mallet, C., Mugica, J., 2019. Imprints of wave climate and mean sea level variations in the dynamics of a coastal spit over the last 250 years: Cap Ferret, SW France. Earth Surf. Process. Landf. 44, 2112–2125. https://doi.org/10.1002/esp.4634.
Neshaei, M.A.L., Biria, H.A., 2013. Impact of Groyne construction on beach; case study Anzali & Astara Coasts. In: 7th National Congress on Civil Engineering, p. 8.
O'Brien, M.P., 1931. Estuary tidal prisms related to entrance areas. Civ. Eng. 1 (8), 738–739.
O'Brien, M.P., 1969. Equilibrium flow areas of inlets on sandy coasts. J. Waterways Harbors Div. 95, 43–52.
Pilkey, O., Wright, H., 1988. Seawalls versus beaches. J. Coast. Res. 41–64.
Ridderinkhof, W., Hoekstra, P., Van Der Vegt, M., De Swart, H., 2016a. Cyclic behavior of sandy shoals on the ebb-tidal deltas of the Wadden Sea. Cont. Shelf Res. 115, 14–26. https://doi.org/10.1016/j.csr.2015.12.014.
Ridderinkhof, W., de Swart, H.E., van der Vegt, M., Hoekstra, P., 2016b. Modeling the growth and migration of sandy shoals on ebb-tidal deltas. J. Geophys. Res. Earth 121, 1351–1372. https://doi.org/10.1002/2016JF003823.
Robin, N., Levoy, F., Monfort, O., Anthony, E., 2009. Short-term to decadal-scale onshore bar migration and shoreline changes in the vicinity of a megatidal ebb delta. J. Geophys. Res. Earth 114. https://doi.org/10.1029/2008JF001207.
Robinet, A., Idier, D., Castelle, B., Marieu, V., 2018. A reduced-complexity shoreline change model combining longshore and cross-shore processes: the lx-shore model. Environ. Model. Softw. 109, 1–16. https://doi.org/10.1016/j.envsoft.2018.08.010.
Roelvink, D., Huisman, B., Elghandour, A., Ghonim, M., Reyns, J., 2020. Efficient modeling of complex sandy coastal evolution at monthly to century time scales. Front. Mar. Sci. 7 https://doi.org/10.3389/fmars.2020.00535.
Roest, B., de Vries, S., de Schipper, M., Aarninkhof, S., 2021. Observed 800changes of a mega feeder nourishment in a coastal cell: five years of sand engine morphodynamics. J. Mar. Sci. Eng. 9, 1–24. https://doi.org/10.3390/jmse9010037.
SHOM - Service Hydrographique et Océanographique de la Marine, 2005. Carte de nature de fond de l'embouchure de la Gironde - De la pointe de la Coubre à la pointe de la Négade, 74. Technical Report.
Sottolichio, A., Castaing, P., 1999. A synthesis on seasonal dynamics of highly-concentrated structures in the Gironde estuary. C. R. Acad. Sci. Ser. II 329, 795–800.
Stéphan, P., Verdin, F., Arnaud-Fassetta, G., Bertrand, F., Eynaud, F., García-Artola, A., Bosq, M., Culioli, C., Suanez, S., Coutelier, C., Bertran, P., Costa, S., 2019. Holocene coastal changes along the gironde estuary (SW France): New insights from the north médoc peninsula beach/dune system. Quaternaire 30, 47–75. https://doi.org/10.4000/quaternaire.11172.
Stive, M.J., Aarninkhof, S.G., Hamm, L., Hanson, H., Larson, M., Wijnberg, K.M., Nicholls, R.J., Capobianco, M., 2002. Variability of shore and shoreline evolution. Coast. Eng. 47, 211–235. https://doi.org/10.1016/S0378-3839(02)00126-6.
Stive, M., de Schipper, M., Luijendijk, A., Ranasinghe, R., de, J.v.T., Aarninkhof, S., van Gelder-Maas, C., de Vries, S., Henriquez, M., Marx, S., 2013. The Sand Engine: a solution for vulnerable deltas in the 21st century? Coast. Dyn. 1537–1546.
Van den Berg, N., Falqués, A., Ribas, F., 2011. Long-term evolution of nourished beaches under high angle wave conditions. J. Mar. Syst. 88, 102–112. https://doi.org/10.1016/j.jmarsys.2011.02.018.
Van Goor, M., Zitman, T., Wang, Z., Stive, M., 2003. Impact of sea-level rise on the morphological equilibrium state of tidal inlets. Mar. Geol. 202, 211–227. https://doi.org/10.1016/S0025-3227(03)00262-7.

Velasquez-Montoya, L., Overton, M.F., Sciaudone, E.J., 2020. Natural and anthropogenic-induced changes in a tidal inlet: morphological evolution of Oregon Inlet. Geomorphology 350, 106871. https://doi.org/10.1016/j.geomorph.2019.106871.

Vitousek, S., Barnard, P.L., Limber, P., Erikson, L., Cole, B., 2017. A model integrating longshore and cross-shore processes for predicting long-term shoreline response to climate change. J. Geophys. Res. Earth 122, 782–806. https://doi.org/10.1002/2016JF004065.

Vos, K., Harley, M.D., Splinter, K.D., Simmons, J.A., Turner, I.L., 2019a. Sub-annual to multi-decadal shoreline variability from publicly available satellite imagery. Coast. Eng. 150, 160–174. https://doi.org/10.1016/j.coastaleng.2019.04.004.

Vos, K., Splinter, K.D., Harley, M.D., Simmons, J.A., Turner, I.L., 2019b. CoastSat: a Google Earth Engine-enabled Python toolkit to extract shorelines from publicly available satellite imagery. Environ. Model Softw. 122, 104528 https://doi.org/10.1016/j.envsoft.2019.104528.

Vos, K., Splinter, K.D., Palomar-Vázquez, J., Pardo-Pascual, J.E., Almonacid-Caballer, J., Cabezas-Rabadán, C., Kras, E.C., Luijendijk, A.P., Calkoen, F., Almeida, L.P., Pais, D., Klein, A.H.F., Mao, Y., Harris, D., Castelle, B., Buscombe, D., Vitousek, S., 2023. Benchmarking satellite-derived shoreline mapping algorithms. Commun. Earth Environ. 4 doi:110.1038/s43247-023-01001-2.

Warrick, J.A., Vos, K., Buscombe, D., Ritchie, A.C., Curtis, J.A., 2023. A large sediment accretion wave along a northern California littoral cell. JGR Earth Surface 128. https://doi.org/10.1029/2023JF007135 e2023JF007135.

Zarzuelo, C., López-Ruiz, A., Ortega-Sánchez, M., 2019. Evaluating the impact of dredging strategies at tidal inlets: performance assessment. Sci. Total Environ. 658, 1069–1084. https://doi.org/10.1016/j.scitotenv.2018.12.227.